Comparison of SNR image quality metrics for remote sensing systems

Robert D. Fiete, MEMBER SPIE
Theodore Tantalo
Eastman Kodak Company
Commercial and Government Systems
1447 St. Paul Street
Rochester, NY 14653-7225
E-mail: robert.fiete@kodak.com

Abstract. Different definitions of the signal-to-noise ratio (SNR) are being used as metrics to describe the image quality of remote sensing systems. It is usually not clear which SNR definition is being used and what the image quality of the system is when an SNR value is quoted. This paper looks at several SNR metrics used in the remote sensing community. Image simulations of the Kodak Space Remote Sensing Camera, Model 1000, were produced at different signal levels to give insight into the image quality that corresponds with the different SNR metric values. The change in image quality of each simulation at different signal levels is also quantified using the National Imagery Interpretability Rating Scale (NIIRS) and related to the SNR metrics to better understand the relationship between the metric and image interpretability. An analysis shows that the loss in image interpretability, measured as ΔNIIRS, can be modeled as a linear relationship with the noise-equivalent change in reflection (NEΔρ). This relationship is used to predict the values that the various SNR metrics must exceed to prevent a loss in the interpretability of the image from the noise. [DOI: 10.1117/1.1355251]

Subject terms: image quality; remote sensing; satellites; digital imaging; imaging systems.

Paper 200024 received Jan. 19, 2000; revised manuscript received July 24, 2000; accepted for publication Oct. 24, 2000.

1 Introduction

The signal-to-noise ratio (SNR) is a common metric used to communicate the image quality and radiometric performance of a remote sensing imaging system. Much confusion has arisen, however, as to the definition that one is using when discussing SNR performance. When a camera designer specifies an SNR value, it is not always clear how that value was calculated and how it relates to the image quality of the system. For example, if an SNR of 30 is quoted for a system design, it is not clear if the image quality is good or bad. It is also possible to quote a high SNR value and a low SNR value for the same system design and imaging conditions if different SNR metrics are used, even though the image quality is the same. This study looks at several SNR metrics used in the remote sensing community and shows their relationship to image quality and image interpretability using high fidelity image simulations. The first step in defining SNR metrics is to review the derivation of the signal and noise terms for remote sensing systems.

1.1 *Signal*

For this analysis, it will be assumed that the remote sensing system consists of a camera with a digital focal plane array that acquires images in the visible spectrum. Figure 1 shows the process by which the final count value in the digital image is derived from the spectral radiance of a ground target illuminated by the sun. The digital count value of each target pixel in the final image is related to the signal produced by the target radiance. Unfortunately, an exact one-to-one relationship between the digital count value and the actual target radiance does not exist, because the count value also contains signal terms from other sources, i.e., the *noise*. Although the signal in the final image is represented in digital counts, the signal for remote sensing system designs is generally calculated as the number of photoelectrons produced by the remote sensing satellite's detector. The mathematical derivation of the expected signal from the target, s_{target}, calculated as the number of photoelectrons produced by the remote sensing satellite's detector, from a target on the ground follows.

The spectral radiant exitance of a blackbody, for a given wavelength of light λ, is given by Planck's equation[1,2]

$$M_{\text{BB}}(\lambda,T)=\frac{2\pi hc^2}{\lambda^5}\frac{1}{\exp(hc/\lambda kT)-1}\quad(\text{W/m}^2\,\mu\text{m}),\quad(1)$$

where T is the temperature of the source in kelvins, $h=6.63\times10^{-34}$ J s, $c=3\times10^8$ m/s, and $k=1.38\times10^{-23}$ J/K. For a Lambertian surface, the spectral radiance from a blackbody is given by

$$L_{\text{BB}}(\lambda)=\frac{M_{\text{BB}}(\lambda,T)}{\pi}\quad(\text{W/m}^2\ \mu\text{m sr}).\quad(2)$$

If the exitance from the sun is approximated by that of a blackbody, then the solar spectral irradiance on a target on the ground can be approximated as

 0091-3286/2001/$15.00

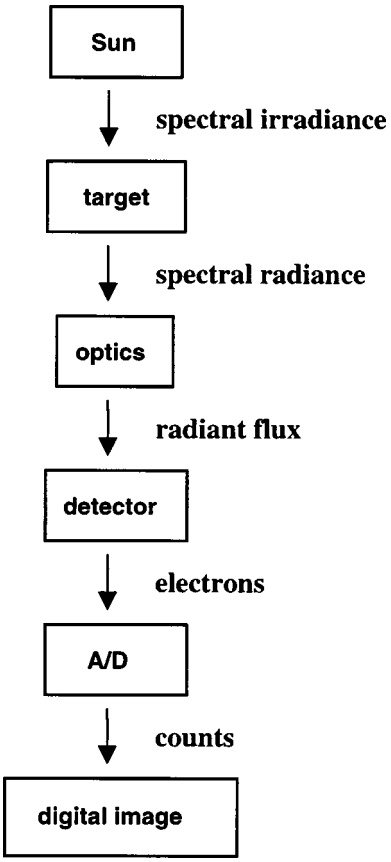

Fig. 1 The process by which the final count value in the digital image is derived from the spectral radiance of a ground target illuminated by the sun.

$$E_{\text{target}}(\lambda) \approx M_{\text{BB}}(\lambda, T_{\text{sun}}) \frac{r_{\text{sun}}^2}{r_{\text{earth-sun}}^2} \tau_{\text{atm}}^{\text{sun-targ}}(\lambda) \times \cos(\phi_{\text{zenith}}) \quad (\text{W/m}^2\ \mu\text{m}), \tag{3}$$

where r_{sun} is the radius of the sun, $r_{\text{earth-sun}}$ is the distance from the earth to the sun, $\tau_{atm}^{\text{sun-targ}}$ is the atmospheric transmittance along the path from the sun to the target, ϕ_{zenith} is the solar zenith angle, and T_{sun} is approximately 5900 K.

The spectral radiance from a Lambertian target at the entrance aperture of the remote sensing satellite is[1,2]

$$L_{\text{target}}(\lambda) = \tau_{\text{atm}}^{\text{targ-sat}}(\lambda) \left\{ \frac{\rho_{\text{target}}(\lambda)}{\pi} [E_{\text{target}}(\lambda) + E_{\text{skylight}}(\lambda)] + \epsilon_{\text{target}}(\lambda) L_{\text{BB}}(\lambda, T_{\text{target}}) \right\} \tag{4}$$

where $\tau_{\text{atm}}^{\text{targ-sat}}$ is the atmospheric transmittance along the path from the target to the satellite, ρ_{target} is the reflectance of the target, ϵ_{target} is the emissivity of the target, and E_{skylight} is the irradiance on the target due to the skylight from atmospheric scattering. Radiometry models, such as MODTRAN, are generally used to calculate L_{target} because the radiometric calculations are dependent on the acquisition geometry and can be complicated.[1,2] Note that the spectral radiance L_{target} is a combination of the solar irradiance that is reflected from the ground target and the blackbody radiance from the target. This analysis will focus on remote sensing in the visible imaging spectrum only, so it will be assumed that the term containing $L_{\text{BB}}(\lambda, T_{\text{target}})$ is negligible compared to the solar irradiance term.

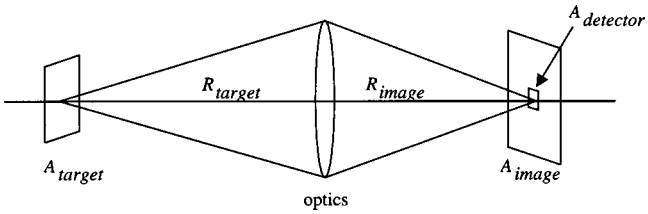

Fig. 2 Imaging system at a distance R_{target} from the target with the focal plane at a distance R_{image} from the camera optics.

Figure 2 illustrates an imaging system at a distance R_{target} from the target with the focal plane at a distance R_{image} from the camera optics. For a polychromatic remote sensing camera where the aperture is small compared to the focal length f, the radiant flux within the spectral passband reaching the entrance aperture of the camera from the target is[1,3]

$$\Phi_{\text{aperture}} = \frac{A_{\text{target}} A_{\text{aperture}}}{R_{\text{target}}^2} \int_{\lambda_{\min}}^{\lambda_{\max}} L_{\text{target}}(\lambda)\, d\lambda = A_{\text{target}} \Omega \int_{\lambda_{\min}}^{\lambda_{\max}} L_{\text{target}}(\lambda) d\lambda \quad (\text{W}), \tag{5}$$

where $\lambda_{\min}$ and $\lambda_{\max}$ define the spectral passband, A_{target} is the area of the target, A_{aperture} is the area of the camera aperture, and Ω is the solid angle encompassing the aperture area. The area of the image, A_{image}, is given by

$$A_{\text{image}} = m^2 A_{\text{target}}, \tag{6}$$

where m is the magnification given by

$$m = \frac{R_{\text{image}}}{R_{\text{target}}}. \tag{7}$$

Thus A_{target} can then be written as

$$A_{\text{target}} = A_{\text{image}} \frac{R_{\text{target}}^2}{R_{\text{image}}^2}. \tag{8}$$

Rewriting the Gaussian lens formula,

$$\frac{1}{R_{\text{target}}} + \frac{1}{R_{\text{image}}} = \frac{1}{f}, \tag{9}$$

in terms of m and R_{image}, where f is the focal length of the optical system, we get

$$R_{\text{image}} = f(m+1). \tag{10}$$

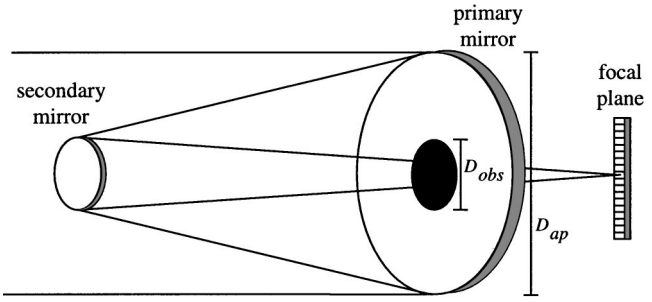

Fig. 3 Telescope design with a primary and a secondary mirror.

Using Eq. (8) and Eq. (10), and multiplying by the transmittance of the optics, τ_{optics}, the radiant flux reaching the image plane is

$$\Phi_{\text{image}} = \frac{A_{\text{image}} A_{\text{aperture}}}{f^2 (m+1)^2} \int_{\lambda_{\min}}^{\lambda_{\max}} L_{\text{target}}(\lambda)\, \tau_{\text{optics}}(\lambda)\, d\lambda. \tag{11}$$

If the size of the target is large compared to the ground instantaneous field of view (GIFOV), then the target is an extended source and $A_{\text{image}} \gg A_{\text{detector}}$, as shown in Fig. 2, where A_{detector} is the area of the detector. The radiant flux on the detector for an extended source is

$$\Phi_{\text{detector}} = \frac{A_{\text{detector}}}{A_{\text{image}}} \Phi_{\text{image}} = \frac{A_{\text{detector}} A_{\text{aperture}}}{f^2 (m+1)^2} \int_{\lambda_{\min}}^{\lambda_{\max}} L_{\text{target}}(\lambda)\, \tau_{\text{optics}}(\lambda)\, d\lambda. \tag{12}$$

For remote sensing cameras, $R_{\text{target}} \gg R_{\text{image}}$; therefore $m+1 \approx 1$ and $f \approx R_{\text{image}}$. If the remote sensing camera uses a telescope design of the general kind sketched in Fig. 3, such as a Ritchey Chretien or a Cassegrain, then the radiant flux on the detector can be written as

$$\Phi_{\text{detector}} = \frac{A_{\text{detector}} \pi (D_{\text{ap}}^2 - D_{\text{obs}}^2)}{4 f^2} \int_{\lambda_{\min}}^{\lambda_{\max}} L_{\text{target}}(\lambda) \times \tau_{\text{optics}}(\lambda)\, d\lambda, \tag{13}$$

or

$$\Phi_{\text{detector}} = \frac{A_{\text{detector}} \pi (1-\epsilon)}{4 (\text{f\#})^2} \int_{\lambda_{\min}}^{\lambda_{\max}} L_{\text{target}}(\lambda)\, \tau_{\text{optics}}(\lambda)\, d\lambda, \tag{14}$$

where D_{ap} is the diameter of the optical aperture, D_{obs} is the diameter of the central obscuration, ϵ is the fraction of the optical aperture area obscured, and f# is the system f number given by

$$\text{f\#} = \frac{f}{D_{\text{ap}}}. \tag{15}$$

The number of photons reaching the detector is

$$n_{\text{detector}} = \frac{A_{\text{detector}} \pi (1-\epsilon)}{4 (\text{f\#})^2} \int_{\lambda_{\min}}^{\lambda_{\max}} \left(\frac{\lambda}{hc} t_{\text{int}} \right) L_{\text{target}}(\lambda) \times \tau_{\text{optics}}(\lambda)\, d\lambda \quad \text{(photons)}, \tag{16}$$

where t_{int} is the integration time of the imaging system. Finally, the signal from the target, measured in electrons generated at the detector, is

$$s_{\text{target}} = \frac{A_{\text{detector}} \pi (1-\epsilon) t_{\text{int}}}{4 (\text{f\#})^2 hc} \int_{\lambda_{\min}}^{\lambda_{\max}} \eta(\lambda) L_{\text{target}}(\lambda) \times \tau_{\text{optics}}(\lambda) \lambda\, d\lambda \quad \text{(electrons)}, \tag{17}$$

where η is the quantum efficiency, which is the average number of photoelectrons generated per incident photon.

1.2 *Noise*

Although the list of all noise sources in a digital remote sensing system is long,[3] only the major contributors will be discussed here.

Random noise arises from elements that add uncertainty to the signal level of the target and is quantified by the standard deviation of its statistical distribution. If the noise contributors are independent and each follows a normal distribution, then the variance of the total noise is the sum of the variances of all the noise contributors.[4] For N independent noise contributors, the standard deviation of the total noise is

$$\sigma_{\text{noise}} = \left(\sum_{n=1}^{N} \sigma_n^2 \right)^{1/2}. \tag{18}$$

For images with large signal, the primary noise contributor is the photon noise, which arises from the random fluctuations in the arrival rate of photons. The photon noise follows a Poisson distribution[4]; therefore, the variance of the photon noise equals the expected signal level s, so that

$$\sigma_{\text{photon}} = \sqrt{s}. \tag{19}$$

When $s > 10$, the Poisson distribution approximates a normal distribution.

The radiance from the target is not the only light that reaches the detector. Scattered radiance from the atmosphere, as well as any stray light within the camera, will produce a background signal superimposed on the target signal at the detector. The background contribution adds an additional photon noise factor to the noise term; thus the photon noise, measured in electrons, is

$$\sigma_{\text{photon}} = (\sigma_{\text{photon target}}^2 + \sigma_{\text{photon background}}^2)^{1/2} = (s_{\text{target}} + s_{\text{background}})^{1/2}. \tag{20}$$

As with the calculation of L_{target}, calculating the atmospheric contribution to the signal is a complicated process.[1,2] Therefore, radiometry models, such as MODTRAN, are generally used to calculate the background radiance component of $s_{\text{background}}$.

When no light is incident on the CCD detector, electrons may still be generated due to the dark noise, σ_{dark}. Although many factors contribute to the dark noise,[3] the principal contributor to σ_{dark} at nominal operating integration times of less than 1 s is the CCD read noise, caused by variations in the detector voltage. The value of σ_{dark} for a digital sensor is usually obtained from test measurements of the detector at a given temperature.

The analog-to-digital (A/D) converter quantizes the signal when it is converted to digital counts. This produces an uncertainty in the target signal, because a range of target signals can produce the same digital count value. The standard deviation of a uniform distribution is $1/\sqrt{12}$; therefore, if the total number of electrons that can be stored at each detector, $N_{\text{well depth}}$, is divided into N_{DR} digital counts, where N_{DR} is the dynamic range in digital counts, then the quantization noise is

$$\sigma_{\text{quantization}} = \frac{N_{\text{well depth}}}{N_{\text{DR}}\sqrt{12}} = \frac{\text{QSE}}{\sqrt{12}}, \tag{21}$$

where QSE is the quantum step equivalence, in electrons per count.

Combining Eq. (19) and Eq. (21) with the dark noise, the system noise can be written as

$$\sigma_{\text{noise}} = \sqrt{s_{\text{target}} + s_{\text{background}} + \sigma^2_{\text{quantization}} + \sigma^2_{\text{dark}}} \quad (\text{electrons}). \tag{22}$$

2 SNR Image Quality Metrics

Many different metrics have surfaced in the remote sensing community over the years to define the SNR. In their basic form, all of the metrics ratio a signal level to a noise level, i.e.,

$$\text{SNR} \equiv \frac{\text{signal}}{\text{noise}}, \tag{23}$$

but differences arise in what is considered *signal* and what is considered *noise*. Most SNR metrics compare the mean target signal with the standard deviation of the noise, so that

$$\text{SNR} = \frac{\text{mean target signal}}{\text{signal deviation}} = \frac{s_{\text{target}}}{\sigma_{\text{noise}}}. \tag{24}$$

This SNR calculation for a remote sensing system design would be straightforward except for the calculation of the target spectral radiance, $L_{\text{target}}(\lambda)$. The target spectral radiance is dependent on the imaging collection parameters, i.e., the solar angle, the atmospheric conditions, and the viewing geometry of the remote sensing system, as well as the target reflectance $\rho_{\text{target}}(\lambda)$.

Assuming that ''typical'' imaging collection parameters will be used to calculate the SNR, the most common difference between SNR metrics is the value used for $\rho_{\text{target}}(\lambda)$. A common assumption is to use the signal from a 100%-reflectance target, given by

$$\text{SNR}_{\rho=100\%} = \left.\frac{s_{\text{target}}}{\sigma_{\text{noise}}}\right|_{\rho_{\text{target}}=100\%}, \tag{25}$$

where the vertical line means ''evaluated at.'' This metric is not very realistic for remote sensing purposes, so values closer to the average reflectance of the earth are used instead. For land surfaces, the average reflectance of the earth between $\lambda_{\min}=0.4$ μm and $\lambda_{max}=0.9$ μm is approximately 15%, but will vary depending on the terrain type, such as soil and vegetation, as well as the season.

Two targets cannot be distinguished from one another in the image if the difference between their reflectance values is below the signal differences caused by the noise. It is therefore beneficial to define the signal in terms of the difference of the reflectance between two targets (or a target and its background),

$$\Delta\rho = \rho_{\text{high}} - \rho_{\text{low}}. \tag{26}$$

The SNR metric for the reflectance difference between the two targets is

$$\text{SNR}_{\Delta\rho} = \frac{s_{\text{target}}|_{\rho_{\text{target}}=\rho_{\text{high}}} - s_{\text{target}}|_{\rho_{\text{target}}=\rho_{\text{low}}}}{\sigma_{\text{noise}}} = \frac{s_{\text{target}}|_{\rho_{\text{target}}=\Delta\rho}}{\sigma_{\text{noise}}}. \tag{27}$$

This SNR metric is used often in the remote sensing community, but the value of $\text{SNR}_{\Delta\rho}$ is dependent on the values chosen for ρ_{high} and ρ_{low}. The value for ρ_{high} is typically used to calculate the photon noise in σ_{noise}.

Another metric commonly used is the noise-equivalent change in reflectance, or NE$\Delta\rho$, which represents the difference in reflectance between two targets that is equivalent to the standard deviation of the noise. It will be difficult, to differentiate two targets that have reflectance differences less than the NE$\Delta\rho$, due to the noise. The NE$\Delta\rho$ can be calculated by solving $\text{SNR}_{\Delta\rho}$ for $\Delta\rho$. If $\Delta\rho$ is independent of λ, then the NE$\Delta\rho$ is simply

$$\text{NE}\Delta\rho = \frac{1}{\text{SNR}_{\Delta\rho}/\Delta\rho} = \frac{\Delta\rho}{\text{SNR}_{\Delta\rho}} = \frac{\sigma_{\text{noise}}}{s_{\text{target}}|_{\rho_{\text{target}}=100\%}}. \tag{28}$$

2.1 *Noise Gain*

Images are usually enhanced using digital image-processing algorithms to improve their interpretability. Processing techniques used to sharpen edges and enhance fine details in an image will also amplify the standard deviation of the noise, σ_{noise}. The SNR metric can allow for the noise amplification by multiplying the noise term by the noise gain G; hence the SNR with the noise gain is given by

$$\text{SNR}_{\text{with noise gain}} = \frac{1}{G}\text{SNR}. \tag{29}$$

For a sharpening filter $h(x,y)$ that is $M \times N$ pixels in size, the noise gain is calculated by

$$G=\frac{\{\Sigma_{x=1}^{M}\Sigma_{y=1}^{N}[h(x,y)]^2\}^{1/2}}{\Sigma_{x=1}^{M}\Sigma_{y=1}^{N}h(x,y)}. \tag{30}$$

Image-processing filters will also correlate the noise, which can significantly affect the interpretability of the image. Scaling the SNR by the noise gain G takes account of the amplification of the noise, but not of the effect that the correlation may have on the interpretability of the image.

2.2 *Frequency-Based SNR Metrics*

The SNR metrics defined above assume that the signal is returned from a large uniform target that produces one radiance value, and therefore no information relating to the signal as a function of spatial frequencies is incorporated. The optical transfer function (OTF) of an imaging system generally decreases to zero as the spatial frequency increases. Thus, the contrast of the higher spatial frequencies will be reduced more than that of the lower spatial frequencies, and the higher spatial frequencies, i.e., the higher detail, may not be perceptible in the noise. The SNR as a function of the spatial frequencies u and v can be calculated by

$$\mathrm{SNR}_{\mathrm{spectral}}(u,v)=\frac{|F(u,v)\,\mathrm{OTF}(u,v)|}{\langle|N(u,v)|^2\rangle^{1/2}}, \tag{31}$$

where $F(u,v)$ is the target spectrum, $N(u,v)$ is the noise spectrum, $|\ |$ denotes the modulus, and $\langle\ \rangle$ denotes the average.

A simplification of the spectral SNR metric can be made if the noise is uncorrelated, i.e., white, and the OTF is a real function. This metric simply weights the spectral SNR and can be calculated by multiplying the SNR by the normalized target spectrum and the modulus of the OTF, i.e., the *modulation transfer function* (MTF) to give

$$\mathrm{SNR}_{\mathrm{spectral(white\ noise)}}(u,v)=\mathrm{SNR}\frac{|F(u,v)|}{|F(0,0)|}\,\mathrm{MTF}(u,v). \tag{32}$$

This SNR metric is generally not practical for designing remote sensing systems, because it is dependent on the target spectrum and produces a functional form of the SNR.

A further simplification can be made to Eq. (32) by assuming that the target spectrum is uniform, so that $F(u,v)=F(0,0)$. The spectral SNR can then be reduced to a single numerical value by calculating the spectral SNR at the highest spatial frequency that can be captured by the digital detector. In other words, this SNR metric multiplies the SNR by the value of the system MTF (which is the modulus of the OTF) at the Nyquist frequencies,[5] defined by

$$u_N\equiv\frac{1}{2p_x} \tag{33}$$

and

$$v_N\equiv\frac{1}{2p_y}, \tag{34}$$

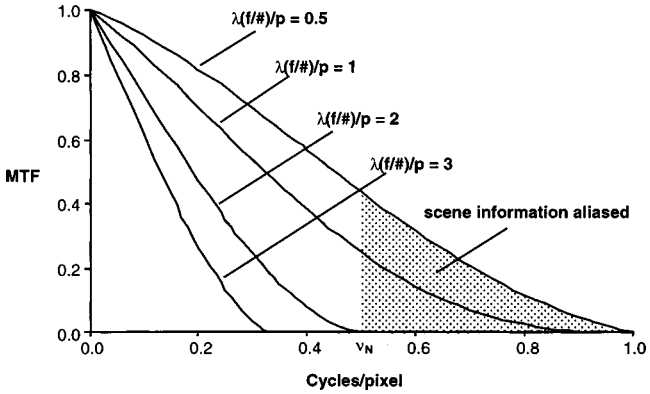

Fig. 4 The system MTF for an incoherent diffraction-limited Ritchey Chretien optical system with a circular aperture and a 10% circular central obscuration for different $\lambda(f\#)/p$ values.

where p_x and p_y are the detector sampling pitches in the x and y directions, respectively. This SNR metric is given by

$$\mathrm{SNR}_{\mathrm{Nyquist}}=\mathrm{SNR}\times\mathrm{MTF}(u_N,v_N). \tag{35}$$

This metric assumes that the MTF at the Nyquist frequency is nonzero, which is not true for systems where u_N or v_N is equal to or higher than the optical passband cutoff frequency, i.e., $\lambda(f\#)/p\geq 2$. If $\lambda(f\#)/p\geq 2$, then the MTF at the Nyquist frequency is zero,[6] as shown in Fig. 4, and the value of $\mathrm{SNR}_{\mathrm{MTF}}$ is always zero, even if the SNR is large and the image quality is very good.

2.3 *Image-Based SNR Metrics*

Some SNR metrics use calculations made from the image data that are collected or simulated. For example, the image scene variability can be compared with the noise variability in the scene by dividing the standard deviation of the image gray-level count values by the standard deviation of the noise in counts, i.e.,

$$\mathrm{SNR}_{\mathrm{scene}}=\frac{\sigma_{\mathrm{image}}(\mathrm{counts})}{\sigma_{\mathrm{noise}}(\mathrm{counts})}. \tag{36}$$

This metric can be useful for testing the performance of algorithms, such as bandwidth compression (BWC), where the scene variance can influence the performance of the algorithm.

Another image-based metric uses the difference between the average count value from a high-reflectance target and the average count value from a low-reflectance target for the signal. The noise is the average of the standard deviation of the counts from the two targets. This SNR is given by

$$\mathrm{SNR}_{\mathrm{scene(high\text{-}low)}}=\frac{\langle\mathrm{counts}\rangle_{\mathrm{high}\text{-}\rho\ \mathrm{target}}-\langle\mathrm{counts}\rangle_{\mathrm{low}\text{-}\rho\ \mathrm{target}}}{(\sigma_{\mathrm{high}\text{-}\rho\ \mathrm{target}}+\sigma_{\mathrm{low}\text{-}\rho\ \mathrm{target}})/2}. \tag{37}$$

This metric assumes that any variability in the count values within the target is due to noise; therefore, large uniform areas of known reflectance values must be present in the image. To improve this measurement, large diffuse reflec-

Table 1 Optics and detector parameters of the Kodak Model 1000 space remote sensing camera.

Optics aperture diameter D_{ap}	44.84 cm
Fraction of aperture area obscured, ϵ	0.06
Focal length f	800 cm
f#	17.84
WFE	0.13λ (at λ=0.6328 μm)
Spectral bandpass, $\lambda_{max}-\lambda_{min}$	0.4 to 0.9 μm
Transmission t_{opt}	0.90
Detector size, $A_{detector}$	12 μm×12 μm
λ f#/p	1.0
Number of TDI stages, N_{TDI}	10, 13, 18, 24, or 32
Line rate	6900 lines/s
Average QE η	0.65
Dynamic range	11 bits (1800 counts)
Well depth $N_{well\ depth}$	153 000 electrons
QSE	85 electrons per count
Dark noise σ_{dark}	70 electrons at 20°C
Number of cross-track detectors	13 816
Altitude	680 km
Look angle	0 deg (nadir)
Sun angle	60 deg
Atmosphere	Mid-lat., summer, 19-km visibility
GSD	1 m

tance panels can be deployed on the ground, with typical values for ρ_{high} and ρ_{low} being 90% and 10%, respectively. Great care must be taken to assure that any variability in the surface reflectance of the panels is well below the detectable limit of the system.

Although image-based SNR metrics are useful in determining the performance of an operational remote sensing system, they are generally not practical for the design of such systems. To accurately compare the performance of different systems, a standard set of images would need to be defined and acquired for all systems. Image-processing enhancements, such as contrast enhancements or edge-sharpening filters, can significantly change the SNR value calculated. Furthermore, sharpening filters can add edge-ringing effects to the image, which can propagate into the uniform areas needed for this calculation. This paper will focus on SNR metrics fundamental to the design and analysis of remote sensing systems.

3 Image Simulations

In order to understand the image quality of remote-sensing imaging satellite designs in terms of the different SNR metrics, an imaging system was modeled and images with different signal levels were simulated.

The design of the Kodak Space Remote Sensing Camera, Model 1000, was modeled for this analysis. The camera is a Ritchey Chretien telescope with a linear CCD detector array. Table 1 lists the optics and detector design parameters as well as the imaging conditions used for the simulations. The Model 1000 camera also contains four multispectral bands, but the focus of this analysis will be on

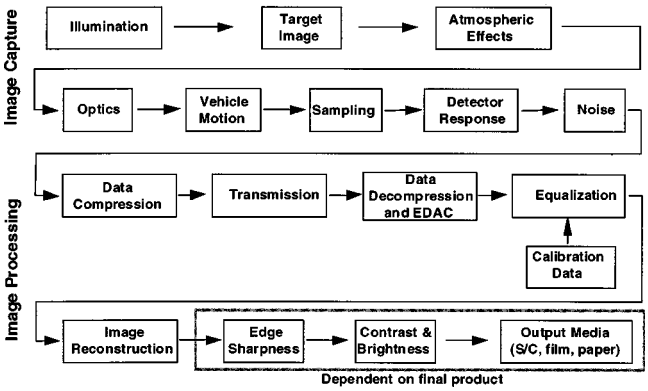

Fig. 5 Image simulation process used for the Kodak space remote sensing camera, Model 1000.

the panchromatic image quality. The camera is designed for a 680-km circular orbit, resulting in a 1-m ground sample distance (GSD).

The detector array is a linear array with time delay and integration (TDI) stages. The TDI process uses multiple detectors in the along-scan direction to collect multiple images of the same ground area as the image moves across the detectors. The multiple images are combined in the detector to improve the effective integration time and SNR. The effective integration time is given by

$$t_{int}=\frac{N_{TDI}}{\text{line rate}}, \tag{38}$$

where the line rate is the number of lines of image data collected per second in the along-scan direction, and N_{TDI} is the number of TDI stages. For the imaging conditions listed in Table 1, the Model 1000 camera would use 10 TDI stages, which gives an effective integration time of 1.45 ms.

The scenes used for the image simulations are panchromatic aerial images collected on high-resolution film with a resolution less than 0.2 m. The images were digitized to an 11-bit dynamic range and a 0.2-m sampling distance. Figure 5 shows the processing steps used to generate the high-fidelity image simulations. MODTRAN 3.5 was used to calculate the radiance terms in s_{target} and $s_{background}$, and a 15% target reflectance value was used to calculate $s_{background}$. The signal level of the image simulations was changed by varying the integration time of the Model 1000 camera. The image smear was held constant, and the QSE was changed as necessary to avoid image saturation at the longer integration times. Noise was added to the images using a Gaussian random number generator having a standard deviation equal to σ_{noise}.

Figure 6 shows a subsection of the image simulations magnified 2× for effective integration times of 10, 5, 1.45, 0.5, 0.1, 0.05, 0.02, and 0.01 ms. Figure 7 shows a subsection of the image simulations magnified 4× for effective integration times of 1.45, 0.5, 0.1, and 0.05 ms, to show the subtle changes in the image quality between these images. Each image simulation was processed with edge-sharpening filters to enhance the detail in the image. The optimal edge-sharpening filter for each image was deter-

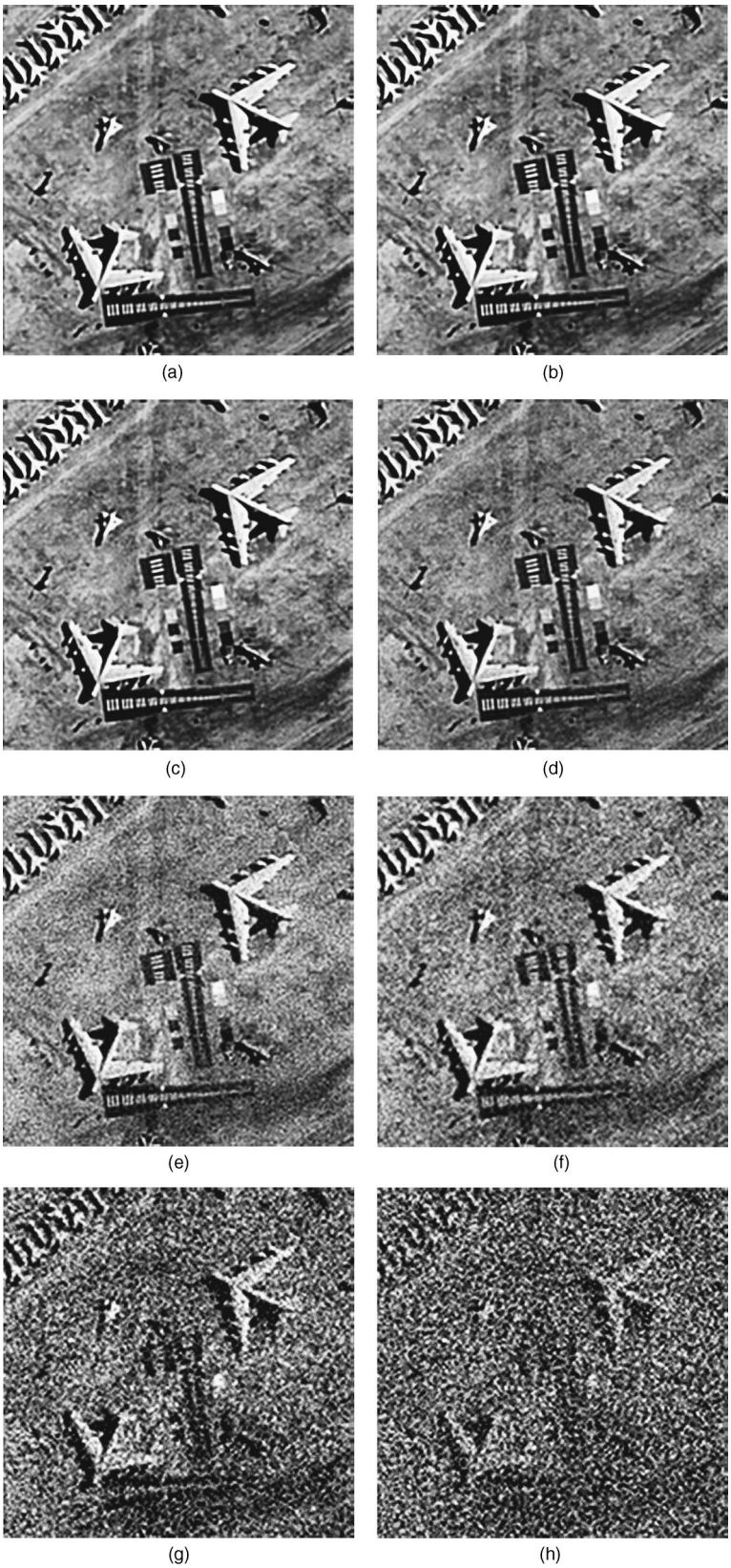

Fig. 6 Image simulations of the Kodak Space Remote Sensing Camera, Model 1000, magnified 2× for effective integration times of (a) 10 ms, (b) 5 ms, (c) 1.45 ms, (d) 0.5 ms, (e) 0.1 ms, (f) 0.05 ms, (g) 0.02 ms, and (h) 0.01 ms.

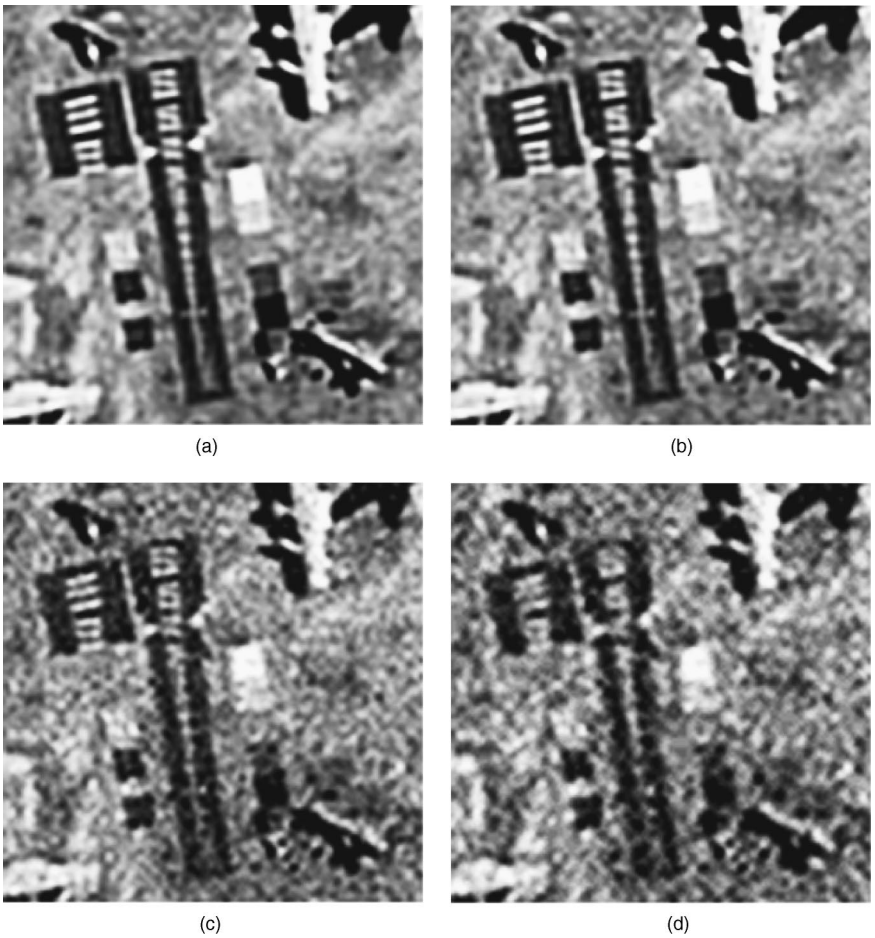

Fig. 7 Image simulations of the Kodak Space Remote Sensing Camera, Model 1000, magnified 4× for effective integration times of (a) 1.45 ms, (b) 0.5 ms, (c) 0.1 ms, (d) 0.05 ms.

mined by processing each image with a series of filters with varying gains and visually inspecting the image to determine the best filter. This filter maximized the visual interpretability of the image, i.e., a filter with a lower gain would render the image too blurry, while a filter with a higher gain would reduce the interpretability due to noise amplification and correlation or to unacceptable edge ringing. The white-noise gain of the filters selected for the image simulations in this study ranged between 1.0 and 5.5. Finally, after edge sharpening, contrast and tonal enhancements were applied to all of the images to optimize the quality.

4 SNR and Image Interpretability

The SNR metrics calculated for each image simulation need to be related to a measure that quantifies the effect that the noise has on a user's ability to interpret the information in the image.

The National Imagery Interpretability Rating Scale (NIIRS)[7] is a 0-to-9 scale that quantifies the interpretability of an image and was initially developed for the reconnaissance community. The scale is an important tool for defining imaging requirements. If more information can be extracted from the image, then the NIIRS rating will increase. Table 2 gives examples of exploitation tasks from the civilian NIIRS that can be accomplished at different NIIRS levels for visible images. Separate military NIIRS scales have been developed for visible, infrared, radar, and multispectral sensor systems, because the exploitation tasks for each sensor type can be very different.

Although NIIRS is defined as an integer scale, ΔNIIRS ratings at fractional NIIRS are performed to measure small differences in image quality between two images. A ΔNIIRS that is less than 0.1 NIIRS is usually not visually perceptible and does not affect the interpretability of the image, whereas a ΔNIIRS above 0.2 NIIRS is easily perceptible. The NIIRS scale is designed so that the ΔNIIRS ratings are independent of the NIIRS rating of the image, e.g., a degradation that produces a 0.2 NIIRS loss in image quality on a NIIRS 6 image will also produce a 0.2 NIIRS loss on a NIIRS 4 image.

The *general image quality equation* (GIQE) was developed as a tool to predict the NIIRS rating of an image given the imaging system design and collection parameters.[8] The GIQE for visible EO systems is

$$\mathrm{NIIRS} = 10.251 - a \log_{10}\mathrm{GSD}_{\mathrm{GM}} + b \log_{10}\mathrm{RER}_{\mathrm{GM}} - 0.656 H_{\mathrm{GM}} - 0.344 \frac{G}{\mathrm{SNR}}, \tag{39}$$

where $\mathrm{GSD}_{\mathrm{GM}}$ is the geometric mean GSD, $\mathrm{RER}_{\mathrm{GM}}$ is the

Table 2 Example exploitation tasks that can be accomplished at different NIIRS levels from the civilian visible-light NIIRS.

NIIRS rating level	Exploitation tasks
0	Interpretability of the imagery is precluded by obscuration, degradation, or very poor resolution.
1	Distinguish between major land use classes (urban, forest, water, etc.). Distinguish between runways and taxiways at a large airfield.
2	Detect large buildings (e.g., hospitals, factories). Identify road patterns, like cloverleafs, on major highway systems.
3	Detect individual houses in residential neighborhoods. Distinguish between natural forest stands and orchards.
4	Detect basketball court, tennis court, volleyball court in urban areas. Identify farm buildings as barns, silos, or residences.
5	Identify tents (larger than two person) at established recreational camping areas. Detect large animals (e.g., elephants, rhinoceros) in grasslands.
6	Identify automobiles as sedans or station wagons. Identify individual telephone/electric poles in residential neighborhoods.
7	Detect individual steps on a stairway. Identify individual railroad ties.
8	Count individual baby pigs. Identify windshield wipers on a vehicle.
9	Identify individual barbs on a barbed wire fence. Detect individual spikes in railroad ties.

geometric mean of the normalized relative edge response (RER), H_{GM} is the geometric mean height overshoot caused by the edge sharpening, G is the noise gain from the edge sharpening, and SNR is the signal-to-noise ratio. The coefficient a equals 3.32 and b equals 1.559 if $\mathrm{RER}_{\mathrm{GM}} \geqslant 0.9$, and a equals 3.16 and b equals 2.817 if $\mathrm{RER}_{\mathrm{GM}} < 0.9$.

The SNR term of the GIQE is calculated using $\mathrm{SNR}_{\Delta\rho}$ in Eq. (27) for $\rho_{\mathrm{high}} = 15\%$ and $\rho_{\mathrm{low}} = 7\%$; thus

$$\mathrm{SNR}_{\mathrm{GIQE}} = \frac{s_{\mathrm{target}}\big|_{\rho_{\mathrm{target}} = \Delta\rho = 8\%}}{\sigma_{\mathrm{noise}}}. \tag{40}$$

The GIQE can be used to predict the change in the image interpretability of each image as the SNR changes. Using the GIQE to predict the ΔNIIRS between two images with different SNRs requires determining the optimal edge-sharpening filter to apply to each image, because the sharpening filter will influence $\mathrm{RER}_{\mathrm{GM}}$, H_{GM}, and G. The image analyst will increase or decrease the strength of the edge-sharpening filter until the interpretability of the image is optimized. If the edge-sharpening filter is not changed, then the predicted change in NIIRS between two different SNRs is

$$\Delta\mathrm{NIIRS} = 0.344G\left(\frac{1}{\mathrm{SNR}_1} - \frac{1}{\mathrm{SNR}_2}\right). \tag{41}$$

In order to better understand the relationship between the various SNR values calculated and image interpretability, a limited ΔNIIRS evaluation was conducted by comparing each of the simulated images with the image simulation with the 10-ms (high-SNR) effective integration time. A total of 66 images were used in the evaluation. The images were rated by four image scientists experienced with ΔNIIRS evaluations. All ratings were performed via a softcopy flicker comparison on a calibrated high-resolution softcopy monitor. Each image scientist was allowed to roam and magnify the images while they were being rated. The experiment was designed so that the presentation order of all comparisons was randomized for each observer.

5 Results and Conclusions

Tables 3–5 list various SNR metrics for each of the image simulations produced. Table 3 lists the SNR metrics calculated without incorporating the system MTF or the noise gain from the enhancement processing. Table 4 incorporates the noise gain, and Table 5 incorporates the system MTF value at Nyquist, both of which reduce the calculated SNR compared to Table 3. Note that the SNR values vary greatly for the same image depending on the SNR metric used. The Model 1000 camera, at an effective integration time of 1.45 ms and at the collection parameters listed in Table 1, can have an SNR value ranging between 3 and 291, depending on the metric used, even though they all represent the same image quality.

Relating the image quality of a system design to NIIRS as a function of SNR is desirable if image interpretability is the driving factor. The average ΔNIIRS rating for each image simulation is shown in Tables 3–5, along with the 95% confidence interval. Standard statistical analysis was performed on the ratings, including an ANOVA analysis to test for outliers (none were found). Figure 8 shows a linear fit between the ΔNIIRS ratings and the $\mathrm{NE}\Delta\rho$ values from Table 3, with the linear relationship given by

$$\Delta\mathrm{NIIRS} = -(0.17 \pm 0.02)\mathrm{NE}\Delta\rho(\%). \tag{42}$$

Table 3 Various SNR metrics for each image simulation.

Image #	1	2	3	4	5	6	7	8
t_{int} (ms)	10	5	1.45	0.5	0.1	0.05	0.02	0.01
ΔNIIRS ratings	0.0±0.0	0.0±0.0	0.0±0.0	0.0±0.0	−0.2±0.1	−0.4±0.1	−1.1±0.2	−1.8±0.2
ΔNIIRS GIQE	−0.01	−0.02	−0.04	−0.08	−0.29	−0.94	−1.3	−1.5
$SNR_{\rho}=100\%$	782	551	291	164	59	35	16	9
$SNR_{\rho}=15\%$	240	167	84	43	12	6	3	1
$SNR_{\Delta\rho\rho_{high}=90\%\ \rho_{low}=10\%}$	656	462	244	137	49	29	13	7
$SNR_{\Delta\rho\rho_{high}=26\%\ \rho_{low}=10\%}$	215	151	77	40	12	7	3	1
$SNR_{\Delta\rho\rho_{high}=15\%\ \rho_{low}=7\%}$	128	89	45	23	6	3	1	1
$NE\Delta\rho_{target}=15\%$	0.06	0.09	0.18	0.35	1.26	2.36	5.64	11.1

Table 4 Various SNR metrics for each image simulation divided by the noise gain.

Image #	1	2	3	4	5	6	7	8
t_{int} (ms)	10	5	1.45	0.5	0.1	0.05	0.02	0.01
ΔNIIRS ratings	0.0±0.0	0.0±0.0	0.0±0.0	0.0±0.02	−0.2±0.1	−0.4±0.1	−1.1±0.2	−1.8±0.2
ΔNIIRS GIQE	−0.01	−0.02	−0.04	−0.08	−0.29	−0.94	−1.3	−1.5
$SNR_{\rho}=100\%$	143	101	53	30	16	10	16	5
$SNR_{\rho}=15\%$	44	31	15	8	3	2	3	1
$SNR_{\Delta\rho\rho_{high}=90\%\ \rho_{low}=10\%}$	120	85	45	25	13	8	13	4
$SNR_{\Delta\rho\rho_{high}=26\%\ \rho_{low}=10\%}$	39	28	14	7	3	2	3	1
$SNR_{\Delta\rho\rho_{high}=15\%\ \rho_{low}=7\%}$	23	16	8	4	2	1	1	0
$NE\Delta\rho_{target}=15\%$	0.34	0.49	0.98	1.92	4.60	8.64	5.64	21.1

Table 5 Various SNR metrics for each image simulation multiplied by the MTF at Nyquist.

Image #	1	2	3	4	5	6	7	8
t_{int} (ms)	10	5	1.45	0.5	0.1	0.05	0.02	0.01
ΔNIIRS ratings	0.0±0.0	0.0±0.0	0.0±0.0	0.0±0.02	−0.2±0.1	−0.4±0.1	−1.1±0.2	−1.8±0.2
ΔNIIRS GIQE	−0.01	−0.02	−0.04	−0.08	−0.29	−0.94	−1.3	−1.5
$SNR_{\rho}=100\%$	48	34	18	10	4	2	1	1
$SNR_{\rho}=15\%$	15	10	5	3	1	0	0	0
$SNR_{\Delta\rho\rho_{high}=90\%\ \rho_{low}=10\%}$	41	29	15	8	3	2	1	0
$SNR_{\Delta\rho\rho_{high}=26\%\ \rho_{low}=10\%}$	13	9	5	3	1	0	0	0
$SNR_{\Delta\rho\rho_{high}=15\%\ \rho_{low}=7\%}$	8	6	3	1	0	0	0	0
$NE\Delta\rho_{target}=15\%$	1.01	1.45	2.88	5.68	20.3	38.1	91.0	180

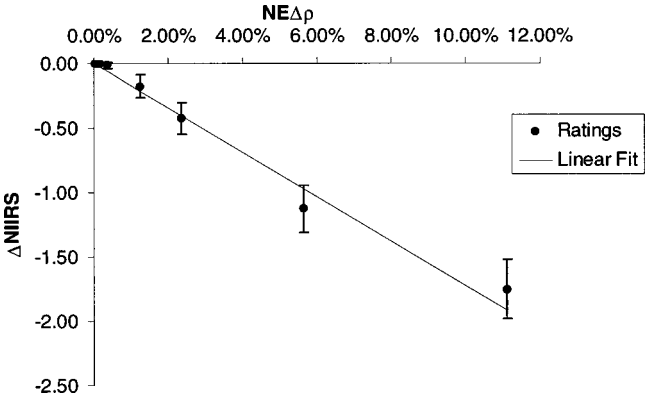

Fig. 8 Linear fit between the ΔNIIRS ratings and the NEΔρ values from Table 3.

This suggests that the relationship between ΔNIIRS and $SNR_{\Delta\rho}$ for the Model 1000 remote sensing camera is simply a linear relationship with the reciprocal of $SNR_{\Delta\rho}$. The GIQE ΔNIIRS predictions, shown in Tables 3–5, are statistically different from the ΔNIIRS ratings greater than −0.2, and they do not fit a linear model. It should be noted that the image scientists commented that the images with NEΔρ>5% from Table 3 were difficult to rate.

Table 6 shows the values of the various SNR metrics that produce a predicted ΔNIIRS of −0.1 using the relationship in Eq. (42). Images will suffer a loss in NIIRS from the noise if the predicted SNR values for a remote sensing system design are not greater that the values shown in Table 6, except for the NEΔρ, which needs to be less than those shown in Table 6. The 95% confidence interval for the values in Table 6 is ±12%. It should be noted that the GIQE predicts a ΔNIIRS of −0.14 for the SNR values shown in Table 6.

Predicting the NIIRS rating for different system designs at various SNRs is difficult because the interaction between the image interpretability and the noise, the MTF, and the enhancement processing is difficult to model. This is especially true when comparing system design concepts that change the MTF. For example, if the $\lambda(f\#)/p$ increases in a system design while the SNR is held constant, then a stronger edge enhancement will be required to enhance the edge sharpness, but this will increase the noise gain that makes the image appear noisier. A similar difficulty at predicting the NIIRS is seen with sparse aperture systems, which require stronger edge enhancement processing, therefore increasing the noise gain. High-fidelity image simulations can be produced for system designs at various SNRs in order to determine an acceptable SNR to build the system at, but image evaluations will still need to be conducted to relate them to NIIRS.

The SNR values calculated in Tables 3–5 and Table 6 can be used as a reference to help understand how each SNR metric relates to image quality by comparing the values with the image simulations and the ΔNIIRS ratings. This reference should be accurate for variations to the imaging conditions used in this study, but will be less accurate for system designs that deviate considerably from the model 1000 remote sensing camera design used in this analysis. It is always important for the designers of remote sensing systems to clearly state the SNR metric that is being used when quoting an SNR value for the system and to understand the relationship of the SNR value to image quality.

Table 6 Values for the various SNR metrics that produce a ΔNIIRS of −0.1 using the evaluation results.

SNR metric	Value	Divided by the noise gain	Multiplied by the MTF at Nyquist
$SNR_{\rho=100\%}$	109	20	6.7
$SNR_{\rho=15\%}$	25	4.7	1.6
$SNR_{\Delta\rho}$:			
ρ_{high}=90%, ρ_{low}=10%	90	17	5.6
ρ_{high}=26%, ρ_{low}=10%	25	4.6	1.5
ρ_{high}=15%, ρ_{low}=7%	14	2.5	0.8
NEΔρ (%): ρ_{target}=15%	0.59	3.2	9.5

Acknowledgments

We would like to thank Jim Mooney, Frank Tantalo, Lana Jobes, Mike Richardson, and Don Vandenburg for their support and helpful discussions.

References

1. J. R. Schott, *Remote Sensing, The Image Chain Approach*, Oxford Univ. Press, New York (1997).
2. R. A. Schowengerdt, *Remote Sensing, Models and Methods for Image Processing*, Academic Press, New York (1997).
3. G. C. Holst, *CCD Arrays, Cameras, and Displays*, SPIE Optical Engineering Press, Bellingham, WA (1998).
4. B. R. Frieden, *Probability, Statistical Optics, and Data Testing*, Springer-Verlag, New York (1983).
5. J. D. Gaskill, *Linear Systems, Fourier Transforms, and Optics*, Wiley, New York (1978).
6. R. D. Fiete, ''Image quality and λFN/*p* for remote sensing systems,'' *Opt. Eng.* **38**, 1229–1240 (1999).
7. J. C. Leachtenauer, ''National imagery interpretability rating scales: overview and product description,'' in *ASPRS/ASCM Annual Convention and Exhibition Technical Papers: Remote Sensing and Photogrammetry*, Vol. 1, pp. 262–272 (1996).
8. J. C. Leachtenauer, W. Malila, J. Irvine, L. Colburn, and N. Salvaggio, ''General image quality equation: GIQE,'' *Appl. Opt.* **36**, 8322–8328 (1997).

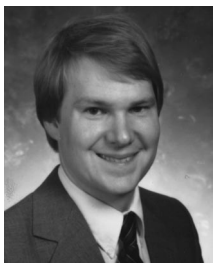

Robert D. Fiete received a BS degree in physics and mathematics from Iowa State University, and an MS and a PhD degree in optical sciences from the University of Arizona. He joined Eastman Kodak Company's Federal Systems Division in 1987 as a project engineer, where he developed image-processing algorithms to model and simulate the image quality of electro-optical imaging system designs. He also developed algorithms for automated focus, target recognition, pseudocolor transforms, multisensor image fusion, and in-scene calibration. Dr. Fiete is currently project manager of the Imaging Systems Analysis group in Kodak's Commercial and Government Systems division. His group's primary responsibility is to assess the image quality of advanced imaging system designs and produce high-fidelity image simulations. Other responsibilities include developing image enhancement algorithms, analyzing system design trades, and conducting psychophysical evaluations.

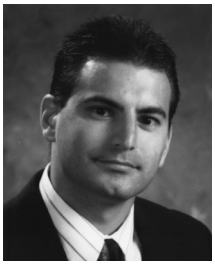

Theodore A. Tantalo is a senior research engineer in the Commercial and Government Systems division at Eastman Kodak Company, joined the company in 1995. Before taking a job in Kodak's Imaging Systems Technology Group, Mr. Tantalo received a BS degree in imaging from the Rochester Institute of Technology and worked in the aerospace/imaging industry. He received an MS in electrical engineering from Pennsylvania State University in 1997 while utilizing his digital image processing and end-to-end optical simulation skills at Kodak. Mr. Tantalo's additional capabilities include advanced digital image algorithm development, image system analysis, reverse engineering, and image quality analysis for entire electro-optical imaging systems.